



FREQUENCY-DOMAIN RECONSTRUCTION OF THE POINT-SPREAD FUNCTION FOR MOVING SOURCES

Sébastien Guérin and Christian Weckmüller
 DLR, German Aerospace Center
 Institute of Propulsion Technology, Engine Acoustics
 Müller-Breslau-Str. 8, 10623 Berlin

ABSTRACT

In beamforming applications where the acoustic source is moving relative to the microphone array, the sidelobes are frequency shifted with respect to the frequency of the source. Furthermore the shape of the beamforming pattern is modified compared to that of the static case at the same position. Provided these two effects are predicted, the DAMAS deconvolution method developed for wind tunnel tests can be modified and applied to aircraft flyovers. While beamforming gives a qualitative information about the noise emission, the deconvolution method enables to quantify separately the level of the sources. In the present paper a solution is given which approximates the point-spread function in the frequency domain. The agreement with simulations is very good for the prediction of the frequency shift and reasonably good for the pattern shape.

1 INTRODUCTION

The determination of the absolute amplitude of acoustic sources with the help of the beamforming technique is the objective of the present study. The special case for which the sources are moving relative to the microphone array is investigated. Acoustic flyover tests of civil aircraft in landing configuration (cf Fig. 1) is the example of application motivating this work. Unlike with the classical beamforming method, the deconvolution method presented by Brooks and Humphreys [1] is a quantitative method. It enables the determination of the absolute level of aerodynamic noise sources. A first modification and application of this method for broadband noise moving sources was presented by Guérin, Weckmüller and Michel [3]. It includes a modification of the point-spread function to take into account the Doppler frequency shift and relies on the assumption that acoustic energy is equally exchanged between neighbouring frequency bands. Since the acoustic signature of modern civil aircraft is dominated by broadband noise (unless the engines are running at high speeds like for take-off) this method provides very good results when applied to real data. The process of analysis between the measurements and the final assessment of the amplitude of the aircraft source components is described in Fig. 2. The following operations are performed until a source breakdown is obtained.

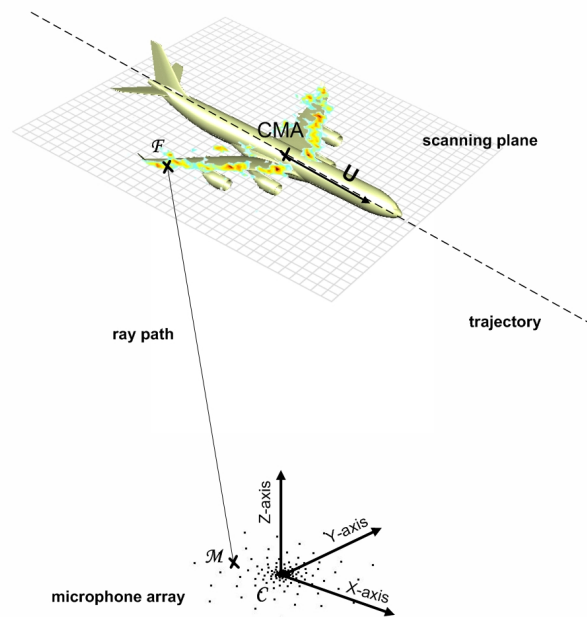


Figure 1: Aircraft flyover.

- The raw data (microphone pressure signals, microphone positions, and aircraft trajectories) are measured and recorded. These data are post-processed as follows.
- The microphone signals and aircraft trajectories are synchronised via GPS time.
- The microphone signals are delayed and summed following the classical rules of beamforming. At this stage of the analysis, acoustic maps of the aircraft are generated. These maps allow only a qualitative description of the noise emission.
- After the point-spread function (or array response) is estimated, the beamforming results are deconvolved in the frequency-domain. The solution is obtained by solving a least-square problem.
- Zones of integration are defined for each one of the potential noise components of the aircraft. The pressure is energetically summed over each zone. The different noise components can be ranked if necessary.

In some measurements, one of the aircraft components (for instance the engines, the landing gear, or the high-lift devices) radiates a tone with an amplitude several decibels higher than broadband noise. In this case the assumption of equal energy transfer between the neighbouring frequency bands is no more valid. This paper proposes a solution to handle with this situation. The solution consists in solving the least-square problem simultaneously over several frequency bands. A necessary condition to apply this technique is that the effects of motion on the point-spread function are well predicted.

The point-spread function represents the array response at focus point \vec{x}_f to an acoustic monopole at position \vec{x}_s . Unlike for static sources, the sidelobes are frequency shifted when $\vec{x}_f \neq \vec{x}_s$. Furthermore, the shape of the pattern is modified compared to that of the static case at the same position. The main focus of the present study is to reconstruct analytically the point-spread function in the frequency domain for moving sources.

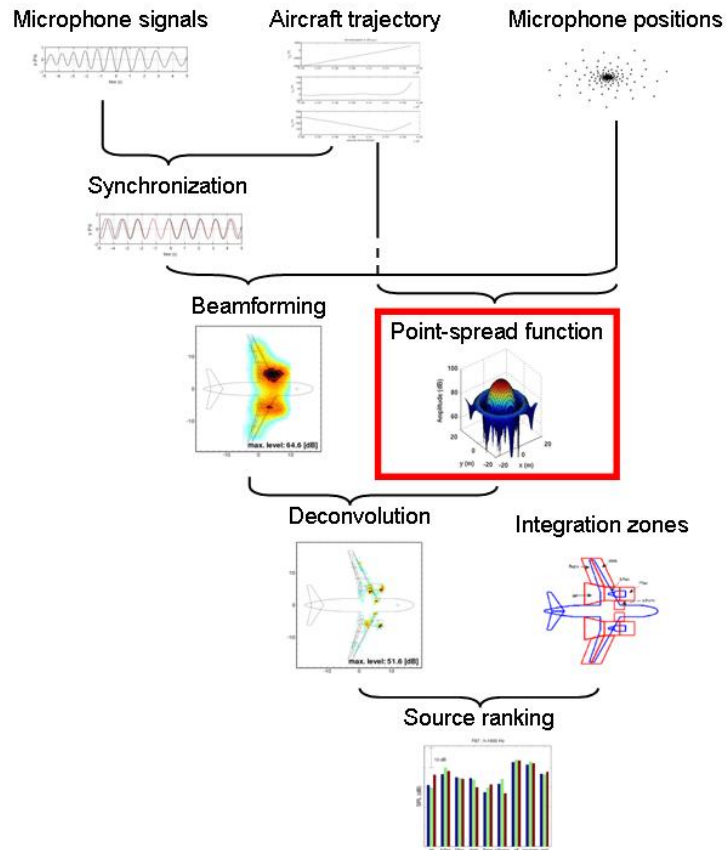


Figure 2: Beamforming analysis of aircraft flyovers.

2 BEAMFORMING

2.1 Time-domain formulation

The analysis begins with the calculation of acoustic maps using the beamforming technique. In order to take into consideration the source motion, the classical time-domain formulation is applied,

$$b_f(t_e) = \sum_{m=1}^M \frac{R_{fm}(t_e)}{R_{\text{ref}}} w_m p_m \left(t_e + \frac{R_{fm}(t_e)}{c_0} \right), \quad (1)$$

where

b_f is the time-domain beamforming solution at focus point \mathcal{F} ,

t_e the emission time,

p_m the signal of the m -th microphone dedopplerised relative to focus point \mathcal{F} ,

R_{fm} the distance between the focus point \mathcal{F} and the m -th microphone,

R_{ref} the distance of normalisation,
 M the number of microphones,
 c_0 the ambient speed of sound, and
 w_m a weighting factor.

Additional corrections for ground reflection, atmospheric attenuation, convective amplification, and so on are not included in Eq. (1). The dedopplerisation supposes that the original microphone signals are resampled. The results presented hereafter were calculated with a linear interpolator. For moving sources, the distance $R_{fm}(t_e)$ is not constant and therefore needs to be new calculated for every time step t_e . The weighting factors w_m are used to change artificially the microphone distribution so that the resolution of the acoustic maps is improved. These factors must verify the following relationship,

$$\sum_{m=1}^M w_m = 1. \quad (2)$$

A spectral representation of the time-domain beamforming solution is obtained by Fourier transformation. At the discrete frequency ω_k , the spectrum $B_f \equiv b_{f,\text{rms}}^2$ is given by

$$B_f \equiv b_{f,\text{rms}}^2(\omega_k) = 2 \langle \hat{b}_f^*(\omega_k) \hat{b}_f(\omega_k) \rangle \quad (3)$$

where \hat{b}_f is the Fast Fourier transform of b_f , the superscript (*) denotes the complex conjugate, and $k = \{1, 2, \dots, K_{\text{FFT}}/2\}$ with K_{FFT} the FFT block size.

2.2 Case of a harmonic point source moving at constant speed

2.2.1 Kinematics

In order to predict the frequency shift of the sidelobes, the case of a harmonic point source moving at constant speed (along a rectilinear trajectory) is considered. A system of coordinates $(\mathcal{O}, \vec{x}, \vec{y}, \vec{z})$ is introduced in which \mathcal{O} represents the origin. The system $(\mathcal{O}, \vec{x}, \vec{y}, \vec{z})$ is orthonormal and positive.

The position \mathcal{M} of a microphone is given by,

$$\overrightarrow{\mathcal{O}\mathcal{M}} = x_m \vec{x} + y_m \vec{y} + z_m \vec{z}. \quad (4)$$

Assuming a trajectory of constant speed \vec{U} , the source position at any time t is simply,

$$\begin{aligned} \overrightarrow{\mathcal{O}\mathcal{S}}(t) &= x_s(t) \vec{x} + y_s(t) \vec{y} + z_s(t) \vec{z} \\ &= (x_0 + U_x t) \vec{x} + (y_0 + U_y t) \vec{y} + (z_0 + U_z t) \vec{z}, \end{aligned} \quad (5)$$

where (x_0, y_0, z_0) corresponds to the source position at time $t = 0$.

The sound pressure measured by the microphone at time t was actually emitted at retarded time (or emission time) t_e ,

$$t_e = t - R_s/c_0. \quad (6)$$

The distance R_s is calculated between the source and the microphone at t_e defined by

$$R_s = \|\overrightarrow{\mathcal{S}(t_e)\mathcal{M}}\|. \quad (7)$$

Let us now simplify the problem. The source is moving on a trajectory parallel to the x -axis, i.e. $U_x = U$, $U_y = 0$, and $U_z = 0$, and at subsonic speed ($U < c_0$). The following relationships are verified [5].

$$R_s = \frac{M_0(x_m - x_0 - Ut) + r_1}{(1 - M_0^2)}, \quad (8)$$

with

$$r_1 = \sqrt{(x_m - x_0 - Ut)^2 + (1 - M_0^2)r_0^2}, \quad (9)$$

$$r_0^2 = (y_m - y_0)^2 + (z_m - z_0)^2, \quad (10)$$

and,

$$M_0 = U/c_0. \quad (11)$$

It can also be demonstrated that R_s , r_1 and $\cos \psi_s$ are related by,

$$r_1 = R_s(1 - M_0 \cos \psi_s). \quad (12)$$

The angle ψ_s is defined between the direction of motion and the direction between the source and the microphone. The cosine of ψ_s is given by the scalar product

$$\cos \psi_s = \frac{\overrightarrow{\mathcal{S}(t_e)\mathcal{M}} \cdot \vec{U}}{\|\overrightarrow{\mathcal{S}(t_e)\mathcal{M}}\| \|\vec{U}\|}. \quad (13)$$

A combination of the previous equations yields also the important relationship

$$\frac{1}{c_0} \frac{dR_s}{dt} = -\frac{M_0 \cos \psi_s}{1 - M_0 \cos \psi_s}. \quad (14)$$

2.2.2 Signal at microphone

Now suppose that the source is harmonic of frequency ω_s . The pressure measured by a microphone is of the form

$$p(t) = \frac{1}{R_s} \cos [\omega_s(t - R_s/c_0)]. \quad (15)$$

The frequency of this microphone signal is changing continuously with time due to motion. Applying Eq. (14), the frequency ω of the signal $p(t)$ can be determined,

$$\omega = \frac{d\phi}{dt} = \omega_s \left(1 - \frac{1}{c_0} \frac{dR_s}{dt} \right) = \frac{\omega_s}{1 - M_0 \cos \psi_s}. \quad (16)$$

The term $Df = 1/(1 - M_0 \cos \psi_s)$ represents the well-known Doppler frequency shift.

2.2.3 Dedopplerised microphone signal

In beamforming, the microphone signals are first dedopplerised with regards to the same focus point \mathcal{F} , and then summed. The dedopplerisation represents a correction of the phase and amplitude of each signal based on the distance R_f between the focus point and the microphone,

$$R_f = \|\overrightarrow{\mathcal{F}(t_e)\mathcal{M}}\|. \quad (17)$$

The signal produced by a harmonic point-source \mathcal{S} dedopplerised with regards to a given focus point \mathcal{F} is

$$\begin{aligned} b_f(t_e) &= \frac{R_f}{R_s} \cos [\omega_s(t_e + R_f/c_0)] \\ &= \frac{R_f}{R_s} \cos [\omega_s(t - R_s/c_0 + R_f/c_0)]. \end{aligned} \quad (18)$$

The frequency ω_f of the dedopplerised signal is given by

$$\omega_f = \frac{d\phi}{dt} = \omega_s \left(1 - \frac{1}{c_0} \frac{dR_s}{dt} + \frac{1}{c_0} \frac{dR_f}{dt} \right). \quad (19)$$

Using Eq. (14), the exact ratio between the frequency ω_s at source and the frequency ω_f at focus point is found to be

$$\frac{\omega_f}{\omega_s} = \frac{1 - 2M_0 \cos \psi_f + M_0^2 \cos \psi_s \cos \psi_f}{(1 - M_0 \cos \psi_s)(1 - M_0 \cos \psi_f)}. \quad (20)$$

If $\psi_s \neq \psi_f$, then $\omega_f \neq \omega_s$. (If $\psi_s = \psi_f$, then $\omega_f = \omega_s$.) This demonstrates why the sidelobes are frequency shifted for moving sources. Eq. (20) can be rewritten as follows.

$$\frac{\omega_f}{\omega_s} = \frac{1 - M_0 \cos \psi_f}{1 - M_0 \cos \psi_s} + \frac{M_0^2 (\cos \psi_f \cos \psi_s - \cos^2 \psi_f)}{(1 - M_0 \cos \psi_s)(1 - M_0 \cos \psi_f)}. \quad (21)$$

The second term of Eq. (21) can be neglected for relative small Mach number M_0 . Then Eq. (20) becomes

$$\frac{\omega_f}{\omega_s} \simeq \frac{1 - M_0 \cos \psi_f}{1 - M_0 \cos \psi_s} = \frac{Df_s}{Df_f}. \quad (22)$$

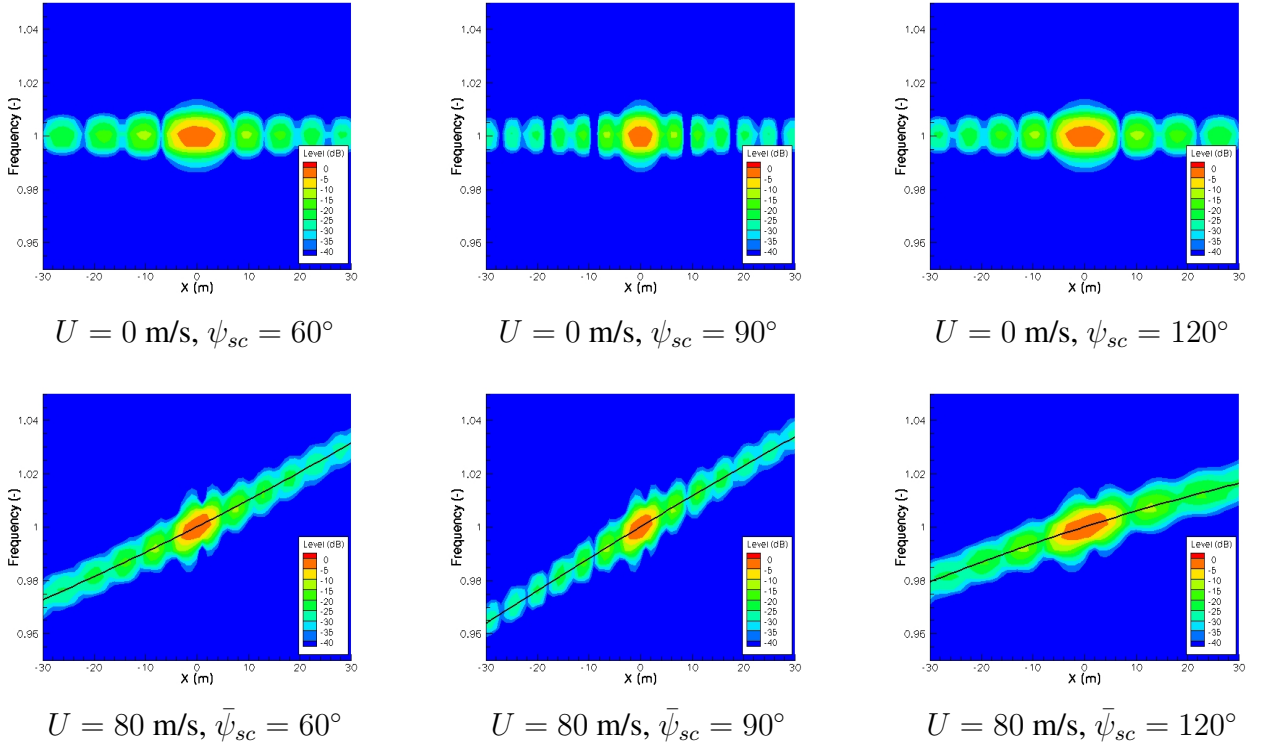


Figure 3: Beamforming solution for a point source at altitude 200 m. The simulations were performed with a harmonic source of frequency 1 kHz detected by a line array of 15 m length composed of 101 equidistant microphones. For the moving case (maps on the bottom), the angle ψ_{sc} between the source and the array center varies approximately between $\bar{\psi}_{sc} - 5^\circ$ and $\bar{\psi}_{sc} + 5^\circ$ with $\bar{\psi}_{sc} = 60^\circ, 90^\circ$, or 120° . The black lines represent the predicted frequency shift determined with Eq. (20). The angle ψ_{fc} between the array center and the middle position of the focus point was applied in the formula.

An example of sidelobe frequency shift is illustrated in Fig. 3 for a point source at 200 m moving at 80 m/s. With motion the sidelobes are changing of frequency which does not happen for the static case. This frequency shift is very well predicted using Eq. (20) when the array center and the middle position of the focus point are taken to determine ψ_s and ψ_f .

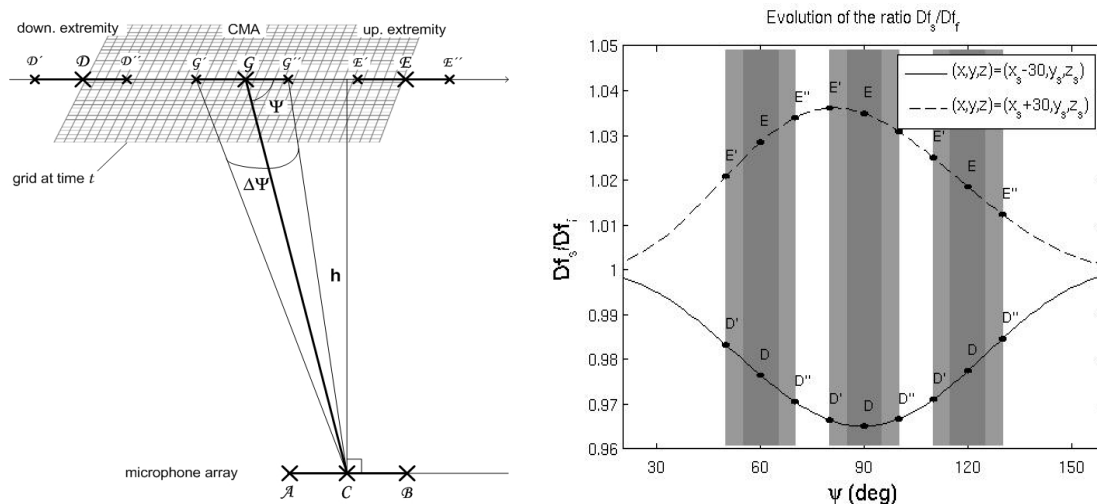


Figure 4: Evolution of the Doppler frequency shift ratio Df_s/Df_f for the two points at the extremities of the scanning plane. The superscripts (') and (") denote the position at the beginning and the end of the time interval, respectively. The middle position (given without superscript) corresponds to the time at which the angle between the center of the scanning plane and the center of the microphone array is equal to 60° , 90° , or 120° . The small and the large grey zones correspond to an aperture of 10° and 20° , respectively.

The Doppler frequency shift is a function of time: this implies that an averaged value is chosen. In Fig. 4, the evolution of the Doppler ratio Df_s/Df_f for the two points at the extremities of the scanning plane is represented in function of the angle ψ_{cg} , where \mathcal{G} represents also the source position here (i.e. $\mathcal{G} = \mathcal{S}$). That ratio is changing rapidly as shown on the graphics on the right-hand side. One can anticipate on the rest of the study and say that the smaller is the aperture (the "shutter speed"), the better can be approximated the point-spread function.

3 RECONSTRUCTION OF THE POINT-SPREAD FUNCTION

3.1 Static sources (without motion)

For an aerodynamic broadband noise source whose position is fixed relative to the microphone array, the square of the pressure amplitude σ of a set of F monopoles modelling the source region can be restored from the output B_f of beamforming by solving the following least square problem [1, 2]

$$C(\sigma) = \sum_{f=1}^F \left(\sum_{s=1}^F H_{fs} \sigma_s - B_f \right)^2 \quad (23)$$

$$\sigma_s \geq 0$$

H is the matrix of point-spread functions. The indices s and f correspond to the source and the focus position, respectively. The following comments are given:

- Eq. (23) is solved separately for each frequency band.
- The monopole sources are assumed to be uncorrelated.
- The number of monopole sources and focus points are equal: the matrix H is square.
- All the values are positive real numbers.

- The constraint $\sigma_s \geq 0$ imposes that the square of the amplitude of the source is positive. (A negative value would not be physical.)

As already mentioned the point-spread function H_{fs} corresponds to the beamforming solution obtained for a single point source of unit amplitude. In other words H_{fs} and $b_{f,\text{rms}}^2$ (defined in Eq. (3)) are strictly equal when the source is a single point source of unit amplitude. One can show that the frequency domain point-spread function for a static source verifies [3]

$$H_{fs}(\omega) = \left| \sum_{m=1}^M w_m \frac{R_{fm}}{R_{sm}} e^{-ik(R_{fm}-R_{sm})} \right|^2. \quad (24)$$

The index m is an index for the microphones, M is the total number of microphones, and $k(= \omega/c_0)$ the wavenumber. For the static case described in legend of Fig. 3, we have compared the beamforming pattern calculated with Eq. (1) and the point-spread function calculated with Eq. (24). The results are shown in Fig. 5 for two angles $\psi_{sc} = 90^\circ$ and 60° . The two solutions agree very well and this for both angles. The discrepancy at the transition between two sidelobes could result from the resampling of the time signals which introduces some noise in the beamforming solution when the relationship between the source frequency ω_s and the resampling frequency ω_{res} does not verify $\omega_f \ll \omega_{res}$ [4].

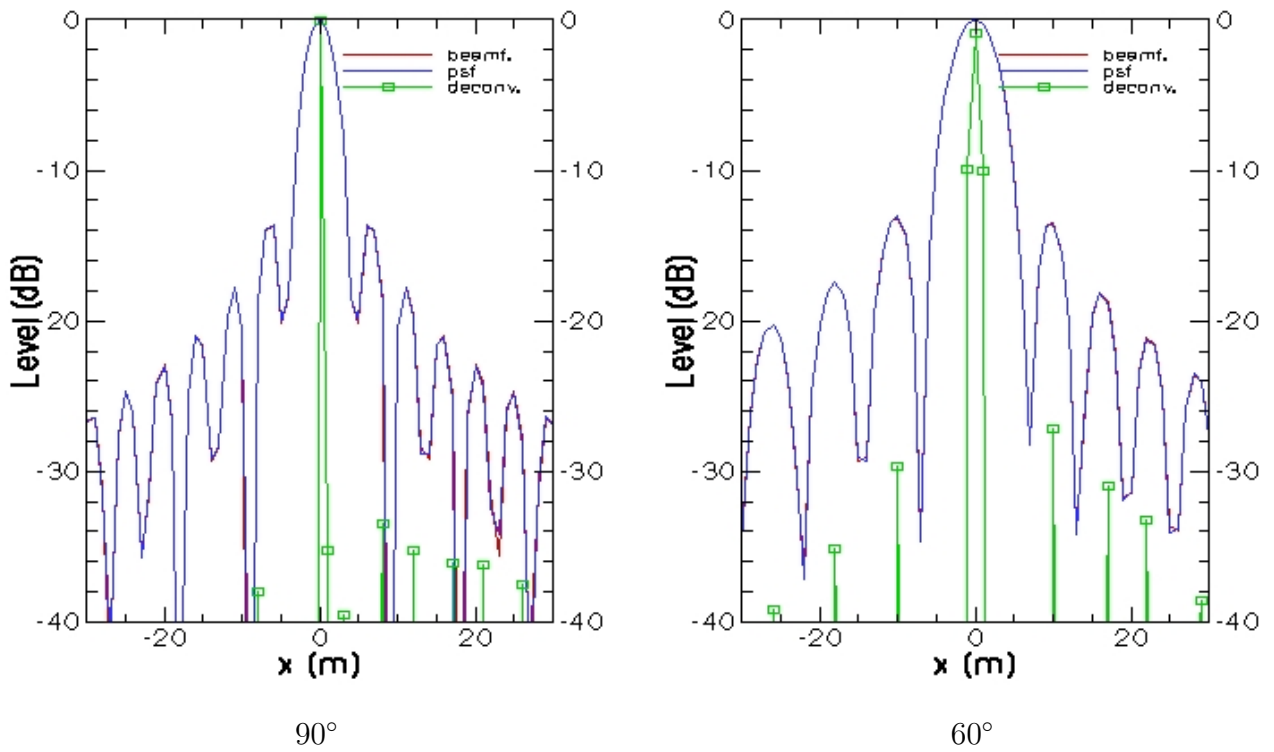


Figure 5: Comparison between beamforming, point-spread function and deconvolution for the case without motion described in legend of Fig. 3.

Using the modified Gauss-Seidel algorithm presented by Brooks and Humphreys [1], the least-square problem of Eq. (23) was solved so that a solution for the source amplitude can be determined. The results are shown in green in Fig. 5. At 90° , the position and the amplitude of the source are both very well recovered. At 60° , the main energy is concentrated at three positions around the source. Clearly the fact that the beamwidth is larger has induced a loss of accuracy in the determination of the source position. The results remain however very satisfactory.

3.2 Moving sources

Because of the frequency shift on the sidelobes, an integration over frequency must be somehow introduced in the problem. The following relationship is verified by beamforming for a problem discretized in space and continuous in frequency,

$$B_f(\omega_f) = \frac{1}{\omega_{res}/2} \int_{\omega_s=0}^{\omega_{res}/2} \sum_{s=1}^F \tilde{H}_{fs}(\omega_s, \omega_f) \sigma_s(\omega_s) d\omega_s, \quad (25)$$

with

$$\tilde{H}_{fs}(\omega_s, \omega_f) = \begin{cases} 0 & \text{if } \frac{\omega_f}{\omega_s} \neq \frac{Df_s}{Df_f} \\ H_{fs}(\omega_s, \omega_f) & \text{if } \frac{\omega_f}{\omega_s} = \frac{Df_s}{Df_f}. \end{cases} \quad (26)$$

The low Mach number hypothesis was considered in Eq. (26) for the estimation of the frequency shift. The main difference to the static case is that the solution must be solved simultaneously in space and frequency for moving sources.

In real applications, the frequencies are multiples of the frequency bandwidth $\Delta\omega_{res} = \omega_{res}/K_{FFT}$. The following relationships are substituted to Eq. (25) and (26)

$$B_f(\omega_f^d) = \sum_{\omega_s^d=\omega_{min}^d}^{\omega_{max}^d} \sum_{s=1}^F \tilde{H}_{fs}(\omega_s^d, \omega_f^d) \sigma_s(\omega_s^d) \quad \text{with } \omega_s^d, \omega_f^d \in [\omega_{min}^d : \omega_{max}^d], \quad (27)$$

with

$$\tilde{H}_{fs}(\omega_s^d, \omega_f^d) = \begin{cases} 0 & \text{if } \omega_s^d \frac{Df_s}{Df_f} \ni \left[\omega_f^d - \frac{\Delta\omega_{res}}{2} : \omega_f^d + \frac{\Delta\omega_{res}}{2} \right] \\ H_{fs}(\omega_s^d, \omega_f^d) & \text{if } \omega_s^d \frac{Df_s}{Df_f} \in \left[\omega_f^d - \frac{\Delta\omega_{res}}{2} : \omega_f^d + \frac{\Delta\omega_{res}}{2} \right] \end{cases} \quad (28)$$

The frequencies ω_{min}^d and ω_{max}^d delimitate the interval of integration for frequency. This interval could correspond for example to the range of frequency over which the sidelobes are shifted. Eq. (23) becomes

$$C(\sigma) = \sum_{\omega_f^d=\omega_{min}^d}^{\omega_{max}^d} \sum_{f=1}^F \left(\sum_{\omega_s^d=\omega_{min}^d}^{\omega_{max}^d} \sum_{s=1}^F \tilde{H}_{fs}(\omega_s^d, \omega_f^d) \sigma_s(\omega_s^d) - B_f(\omega_f^d) \right)^2. \quad (29)$$

$\sigma_s \geq 0$

The amplitude of the point-spread function is now approximated by

$$H_{fs}(\omega) = \left| \sum_{m=1}^M w_m \frac{r_{mf}}{r_{ms}} e^{ikDf_{ms}(r_{mf}-r_{ms})} \right|^2. \quad (30)$$

Compared to Eq. (24), the source wavenumber is replaced by the wavenumber of the signal arriving at the microphones. This solution is better than that proposed by Guérin et al. [3] in which the Doppler frequency shift factor was taken between the source and the array center.

For our test case, the simulated and the approximated point-spread functions are compared in Fig 6. The patterns corresponding to beamforming were extracted along the black lines drawn in Fig. 3.

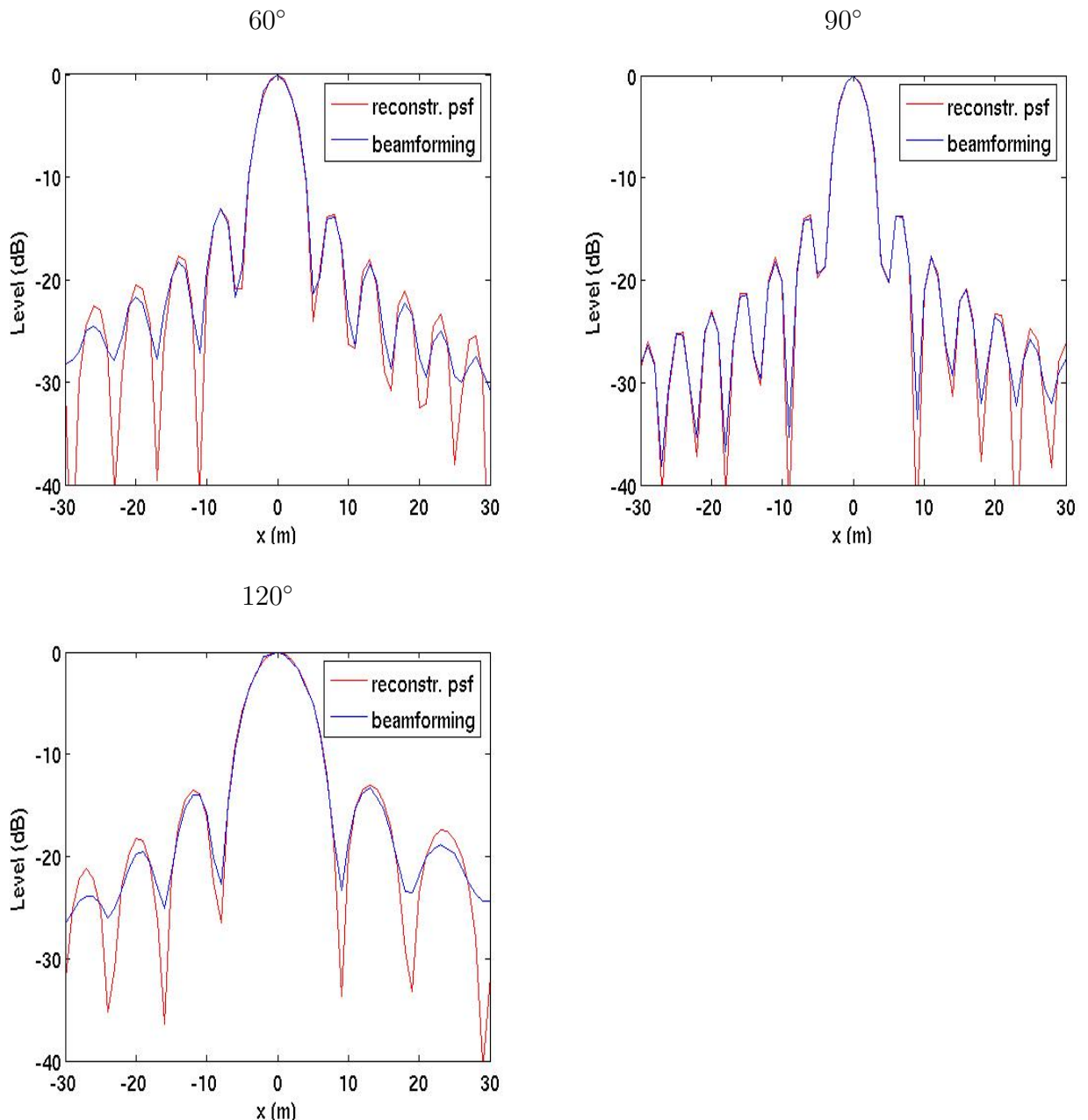


Figure 6: Frequency-domain reconstruction of the point-spread function for our reference example with motion.

The main lobe is very well reconstructed at the three angles. The number of sidelobes and their positions are correctly predicted too, but their amplitude can be underestimated. It appears that energy is slightly smeared between the sidelobes. As a conclusion, some error is introduced when the solution of the point spread function in the frequency domain for moving sources is analytically calculated using Eq. (30).

Keeping that error in mind, the method of deconvolution given by Eq. (29) was applied to the present test case. The results are shown in Fig. 7 for $\psi = 60^\circ$. One observes that the source is not as well recovered as for the static case. However the results are so that most of the energy is concentrated in the vicinity of the source which is encouraging.

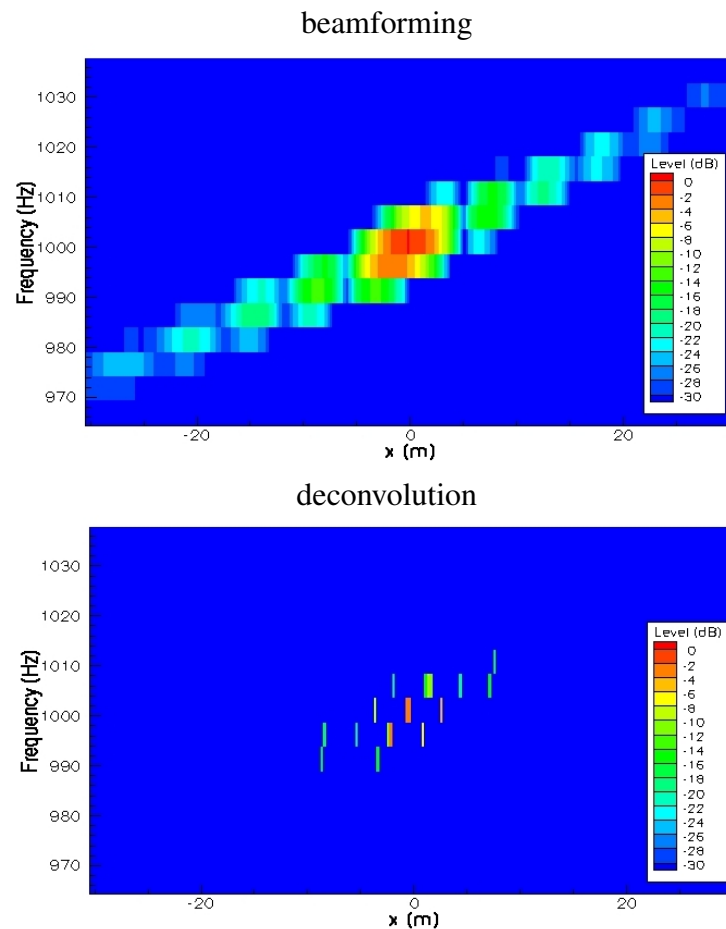


Figure 7: Beamforming vs deconvolution (moving case at 60°).

4 CONCLUSIONS

In order to determine the amplitude of the tonal source when it moves, the DAMAS method was adapted so that now the frequency shift on the sidelobes is taken into account in the formulation of the least-square problem. The modification of the beamforming pattern related to motion was also accounted for. At the end, the problem could be solved at the expense of an increase of the computing time and need in memory. Further testing with real data is necessary to validate the method.

REFERENCES

- [1] T.F. Brooks and W.M. Humphreys. A deconvolution approach for the mapping of acoustic sources (damas) determined from phased microphone arrays. Manchester, UK, 10-12 May 2004. 10th AIAA/CEAS Aeroacoustics Conference. AIAA Paper 2004-2954.
- [2] R.P. Dougherty. Extensions of DAMAS and benefits and limitations of deconvolution in beamforming. Monterey, California (USA), 23-25 May 2004. 11th AIAA/CEAS Aeroacoustics Conference. AIAA Paper 2005-2960.
- [3] S. Guérin, C. Weckmueller, and U. Michel. Beamforming and deconvolution for aerodynamic sources in motion. Berlin, Germany, 21-22 November 2006. First Berlin Beamforming Conference (BeBeC).

- [4] G.P. Howell, A.J. Bradley, M.A. McCormick, and J.D. Brown. De-dopplerization and acoustic imaging of aircraft flyover noise measurements. *Journal of Sound and Vibration*, 105(1):151–167, 1986.
- [5] M. Morse and K.U. Ingard. *Theoretical acoustics*. Princeton edition, 1986. reprinted.